Physica A 560 (2020) 125104

Contents lists available at ScienceDirect

Physica A

journal homepage: www.elsevier.com/locate/physa

Thermodynamic properties of SnO_2/GaAs core/shell nanofiber

M. Kria [a], K. Feddi [b,c,1], N. Aghoutane [a,1], M. El-Yadri [a,1], L.M. Pérez [d,1], D. Laroze [d,*,1], F. Dujardin [e,1], E. Feddi [a,*,1]

[a] Group of Optoelectronic of Semiconductors and Nanomaterials, ENSET de Rabat, Mohammed V University in Rabat, Morocco
[b] EIMIS Laboratory, FST, University Abdelmalek Essadi, Tanger, Morocco
[c] Renewable Energy and Advanced Materials Laboratory, International University of Rabat, Morocco
[d] Instituto de Alta Investigación, CEDENNA, Universidad de Tarapacá, Casilla 7 D, Arica, Chile
[e] Université de Lorraine, LCP-A2MC, 57000 Metz, France

ARTICLE INFO

Article history:
Received 23 March 2020
Received in revised form 1 July 2020
Available online 22 August 2020

Keywords:
Core – shell
Nanofiber
Heat capacity
Entropy
Helmholtz energy

ABSTRACT

We provide a comprehensive computational investigation concerning the effects of confinement and temperature on the thermodynamic properties of cylindrical core/shell quantum dots with a large band offset. This model can also be applied to hollow cylindrical quantum dots or nanofibers. Within the framework of the effective mass approximation, we solve the Schrödinger equation analytically in two bands model, determining the energies of all excited states. Following Boltzmann–Gibbs distribution and introducing the canonical partition function, energy states are used to evaluate the thermodynamic properties: the mean energy, heat capacity, entropy, and Helmholtz free energy. Our numerical calculation shows that all thermodynamic properties depend on the temperature, the size of the dot, and the shell thickness. According to our numerical results, it is found that in the narrow shell case, the heat capacity shows a Schottky-like anomaly at low temperatures, but this effect disappears for small values of core radius. Another important conclusion, is that the determination of the Helmholtz free energy makes it possible to predict the thermodynamic stability of quantum dots. We also show that the competition between the temperature, the core dimension, and the shell thickness influences the thermodynamic stability. Despite the simplicity of our approach, our study can be considered as a useful information source and as an excellent qualitative indicator for understanding the thermodynamic properties of quantum dots.
© 2020 Elsevier B.V. All rights reserved.

1. Introduction

In recent years, investigations of the thermodynamic properties of semiconductor nanomaterials are in the spotlight of many experimental and theoretical types of researches. In addition to their quantum properties related to the geometrical confinement, growth methods and nature of the materials also present some interesting thermodynamic properties [1–7]. It is worth mentioning that recently, scientists can control the number of electrons in a Quantum Dot (QD) by adjusting shape or degree of confinement [8]. In such a situation, the physical and structural properties are modified because of the quantum confinement of the charge carriers. The quantification of energy levels and the change in density of

* Corresponding authors.
E-mail addresses: dlarozen@uta.cl (D. Laroze), e.feddi@um5s.net.ma (E. Feddi).
[1] All the authors contribute to the manuscript in active form.

https://doi.org/10.1016/j.physa.2020.125104
0378-4371/© 2020 Elsevier B.V. All rights reserved.

occupation give to these structures additional optoelectronic properties and influence the thermodynamic properties of these nanomaterials.

Among the most promising geometries, we cite the quantum nanowires with cylindrical symmetry. These structures admit appealing properties for optoelectronic applications and energy harvesting by the thermoelectric phenomenon. Indeed, Wagner and Elliss [9] have grown silicon nanowires with small diameters using the MBE technique. The same process allows obtaining other nanofibers by manipulating several combinations of II–IV, IV–VI, and III–V semiconductors [10–18]. More advanced techniques have made possible to dress these rods with another semiconductors, thus achieving a new generation of cylindrical core/shell with different band offsets structures [19–25]. With this bandgap engineering, new nano-devices are realized according to needs in various areas such as the single-photon source for cryptography and photonic quantum information, quantum light-emitting diodes, solar cells, energy storage, and many other applications mainly in medicine and biology [26–28].

To our knowledge, studies relating to the thermal properties of QDs remain very few, whether from a theoretical or experimental point of view. In what follows, we recall the most important of them, hoping that this will help understand different phenomena generated during this kind of structure. The most impressive studies existing in the literature show that the conclusions about the thermal features in the low-dimensional structures are not unanimous. Indeed, the experiment on the Si and SiGe nanowires showed a significant enhancement in thermoelectric properties [4,5], but, in the case of $BiTe_3$ and InSb nanowires, a decrease in thermoelectric properties has been observed [29–31]. However, Hu et al. [7] found a drastic reduction in the thermal conductivity of SiGe core–shell nanowires.

From the theoretical point of view, numerous works are interested in the determination of thermoelectric properties of core–shell nanowires. We cite the study developed by De Groote et al. [1], which is considered among the first attempts in this topic. They have determined the magnetization, the specific heat, and the magnetic susceptibility of two electrons by solving the Schrödinger equation and considering the spin term. Their study shows that the susceptibility and the heat capacity present peaks at low temperatures. This enhancement was attributed to the increasing of Lande factor. Nguyen and Peeters [32] have determined the thermodynamic properties and magnetic susceptibility taking into account the e–e interactions. B. Boyacioglu and Chatterjee [33] have assessed the effect of bidimensional confinement on the thermodynamic properties. They have analyzed the heat capacity and entropy of GaAs quantum dot in the magnetic field by considering Gaussian quantum confinement. Their model shows that at low temperature, the heat capacity C_v presents a peak structure as observed in the two levels system. This phenomenon is known in the literature as *Schottky anomaly*. Besides, their calculations show that C_v tends to a saturation value of $2k_B$ with increasing temperature. They have also demonstrated that the heat capacity depends on the nature of the confinement. The thermal and magnetic properties of cylindrical quantum dot have been studied using a parabolic confinement potential [34,35]. The authors have demonstrated the existence of a region of magnetic field and temperature from which no change in specific heat was observed. They have also demonstrated the impact of the Rashba effect on the thermodynamic behavior of an InSb QD submitted to a magnetic field. The two authors highlighted the Schottky-like anomaly of the heat capacity at low temperature and demonstrated that Rashba spin–orbit interaction affects the magnetic properties considerably. Khordad and Sedehi [36] have studied the thermodynamic properties of GaAs double ring-shaped quantum dot in the magnetic field at low and high temperatures. They have shown that, at low temperatures, the entropy increases monotonically independently of the magnetic field strength, whereas it depends on the magnetic field for high temperatures. However, their numerical calculations have shown that the heat capacity and magnetic susceptibility present peaks at low temperatures. The behavior of the magnetic susceptibility shows a transition between diamagnetic and paramagnetic for $T < 4$ K. More recently, Nammas et al. [37,38] have published two interesting theoretical studies concerning the thermodynamic properties of two and few electrons in quantum dots where an harmonic potential describes the confinement. They have shown that the mean energy increases slowly at low temperatures, but it increases rapidly as the temperature increases. At low temperatures, the heat capacity increases very quickly, and then it saturates with a further rise in temperature as what happens in bulk materials. In the magnetic field, the effect of confinement shape on both the thermodynamic and transport properties of GaAs quantum dot has been studied more recently [39]. It has been concluded that for low confinement, the mean energy depends strongly on the shape. At the same time, it is almost independent of shape for strong confinement; the heat capacity is found to be independent of the shape and the depth of the confinement potential at very low temperatures. The behavior of heat capacity undergoes a paramagnetic–diamagnetic transition at a critical value of the magnetic field. Thermal properties of an electron gas in a toroidal quantum dot in the presence of a magnetic field has been treated in the effective mass approximation and using the canonical ensemble approach [40]. This analytical calculation demonstrates the existence of Aharonov–Bohm oscillations and Schottky-like anomaly at low temperatures. In a recent investigation, the Dresselhaus and Rashba effects on thermodynamic properties of two-electron interactions in quantum dot under a magnetic field are studied. It has been shown that the heat capacity has two peaks attributed to the singlet–triplet transition point. It also observed that the Coulomb interaction diminishes (enhances) the heat capacity at low (high) temperature. They have also demonstrated that the Dresselhaus effect increases the heat capacity while the Rashba spin–orbit interaction reduces the heat capacity [41].

All these works have demonstrated that the thermal properties undergo significant changes with confinement. To date, there has been no study regarding to the thermodynamic properties of cylindrical core/shell or hollow quantum dots. In this study, we have investigated the thermodynamic properties in this kind of structures using an infinite potential confining. The paper is organized as follows: in Section 2, we describe the basic theory performed in the framework of

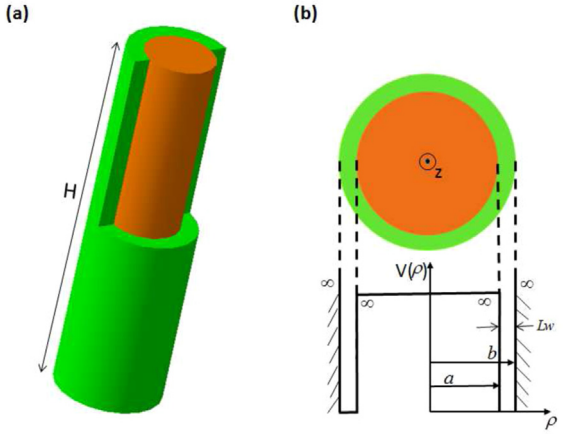


Fig. 1. (a) Pictorial view of the hollow cylindrical structure used in the present study, (b) band offsets representation of the lateral confinement, where a and b are the radii of core and shell materials, respectively, and $L_w = b - a$ is the well thickness.

the effective mass approximation, and we compare their behavior with those obtained in a simple cylindrical quantum dot. Energy levels of ground and excited states are determined numerically and used to obtain all thermodynamic properties by considering the canonical ensemble approach. The numerical results and discussion are provided in Section 3. Finally, brief conclusions are presented in Section 4.

2. Background theory

2.1. Determination of the energy levels

Let us consider the structure indicated in Fig. 1 which corresponds to a cylindrical core/shell quantum dot, such that H is the height, a and b are the inner and outer radius, respectively. We assume that the height is larger than the outer radius ($H \gg b$), but not quite long in order to have a three dimensional confinement. We suppose that our structure is characterized by a large band offset between core and shell materials, such in SiO_2/Si ($E_g^{SiO_2} = 8.9$ eV and $E_g^{Si} = 1.15$ eV) [42], CdS/HgS $\left(E_g^{CdS} = 2.5 \text{ eV and } E_g^{HgS} = 0.5 \text{ eV}\right)$ [43], SnO_2/GaAs ($E_g^{SnO_2} = 3.6$ eV and $E_g^{GaAs} = 1.42$ eV) [44] or SiO_2/GaAs ($E_g^{SiO_2} = 8.9$ eV and $E_g^{GaAs} = 1.42$ eV) [45]. The structure is surrounded by a dielectric medium with large band gap. Let us also recall that the effective mass is a tensor whose elements traduce the fact that the effective mass admits different values according to the different directions [46]. For the materials with a direct gap as in the case of (III–V) semiconductors, the extremum of the conduction band is localized at the center of the Brillouin zone Γ at $k = 0$. In this case, the dispersion relation E(k) is considered as parabolic. Consequently, the effective mass is a scalar independent of the direction. In the effective-mass and two parabolic band approximations, the Hamiltonian of an electron (e) in cylindrical coordinates (ρ, φ, z) writes as:

$$\mathcal{H} = -\frac{\hbar^2}{2m_e^*(T)}\left(\frac{\partial^2}{\partial\rho_e^2} + \frac{1}{\rho_e}\frac{\partial}{\partial\rho_e} + \frac{1}{\rho_e^2}\frac{\partial^2}{\partial\varphi_e^2} + \frac{\partial^2}{\partial z_e^2}\right) + V_w^e(r_e), \tag{1}$$

where r_e is the electron position from the center of the cylinder and $m_e^*(T)$ is its temperature dependent effective mass, which can be described by the following relation [47,48]

$$m_e^*(T) = m_0\left[1 + 7.51\left(\frac{2}{E_g(T)} + \frac{1}{E_g(T) + \Delta_0}\right)\right]^{-1} \tag{2}$$

where m_0 is the free electron mass and $\Delta_0 = 0.341$ eV is the spin–orbit splitting of GaAs. Here, $E_g(T)$ is the temperature dependent GaAs band gap at the center Γ of the Brillouin zone. It can be expressed by the relation [47–49]

$$E_g(T) = 1.519 - \frac{5.4 \times 10^{-4}T^2}{T + 204}, \tag{3}$$

which is measured in meV. Besides, $V_w^e(r_e)$ is the geometrical confinement potential, which is defined as zero inside the shell region and infinite elsewhere. Due to the symmetry of the problem, the total confinement can be considered as the sum of radial part $V_1^e(\rho_e)$ and longitudinal potentials $V_2^e(z_e)$. Consequently, the potential can be written as

$$V_w^e(r_e) = V_1^e(\rho_e) + V_2^e(z_e). \tag{4}$$

Let us remark that in the case of the large band offsets such as in SnO_2/GaAs and SiO_2/GaAs, the electron wave function is primarily localized in the shell region characterized by a thickness $L_w = b - a$. Thus its radial probability density is predominant in the shell with low extensions into the core and vanishes at the border of the external region. In these circumstances, one can consider that the limit of infinite potential can be a good approximation. Some preliminary results confirm this hypothesis. For more details, see Appendix. We also note that this model can be applied correctly in nanofibers or quantum wire structures with a hollow core. Nevertheless, this approximation becomes questionable and even invalid for low band offsets. Under these considerations, the approximation of infinite barriers can be written as:

$$V_w^e(\rho_e) = \begin{cases} 0 & \text{for} \quad a \le \rho_e \le b \\ \infty & ; \quad \text{otherwise} \end{cases} \tag{5}$$

$$V_w^e(z_e) = \begin{cases} 0 & \text{for} \quad |z_e| \le H/2 \\ \infty & ; \quad \text{otherwise} \end{cases} \tag{6}$$

The energy and the wave function are given by the resolution of Schrödinger equation $\mathcal{H}\Psi_e(\rho_e, \varphi_e, z_e) = E^e\Psi_e(\rho_e, \varphi_e, z_e)$, we remark that the Hamiltonian of the system can be written us a sum of the two independent part:

$$\left(\mathcal{H}(\rho_e, \varphi_e) + \mathcal{H}(z_e)\right)\Psi_e(\rho_e, \varphi_e, z_e) = E^e\Psi_e(\rho_e, \varphi_e, z_e)\right) \tag{7}$$

As consequence, the wave function can be expressed as a product of the two independent parts:

$$\Psi_e(\rho_e, \varphi_e, z_e) = f_e(\rho_e, \varphi_e)\, g_e(z_e) \tag{8}$$

and the energy is determined by the sum: $E^e = E_{mn} + E_l$, where E_{mn} is the eigen value of the Schrödinger equation $\mathcal{H}(\rho_e, \varphi_e)f_e(\rho_e, \varphi_e) = E_{mn}f_e(\rho_e, \varphi_e)$. We recall that the wave function obtained by the resolution of this equation is a linear combination of Bessel functions $J_m(k_{mn}\,\rho_e)$ and $Y_m(k_{mn}\,\rho_e)$ of the first and the second kind, respectively [50]:

$$f_e(\rho_e, \varphi_e) = N_1 J_m(k_{mn}\,\rho_e) + N_2\, Y_m(k_{mn}\,\rho_e) \tag{9}$$

where N_1 and N_2 are normalization constants obtained by boundary and normalization conditions of the wave functions, m is the order of Bessel radial functions. It is worth mentioning that in our case, the radial wave function must vanish at the inner ($\rho_e = a$) and outer ($\rho_e = b$) radial borders as well as at the top and bottom of the cylinder. These conditions lead to the transcendental equation [20]:

$$|J_m(k_{mn}\,a)Y_m(k_{mn}\,b) - Y_m(k_{mn}\,a)J_m(k_{mn}\,b)| = 0 \tag{10}$$

where k_{mn} is the nth root of Bessel functions $J_m(k_{mn}\,\rho_e)$ and $Y_m(k_{mn}\,\rho_e)$. The eigenenergies corresponding to the radial Schrödinger equation is $E_{mn} = k_{mn}^2$. Also, in the z-direction, the Schrödinger equation corresponds to an infinite square well

$$\left(-\frac{\hbar^2}{2m_e^*(T)}\frac{\partial^2}{\partial z_e^2} + V_w^e(z_e)\right) g_e(z_e) = E_l g_e(z_e), \tag{11}$$

where the odd eigenfunctions are given by:

$$g_e(z_e) = \sin\left(\frac{l\,\pi\, z_e}{H} + \frac{l\,\pi}{2}\right) \tag{12}$$

and the corresponding quantified energy eigenvalues are $E_l = \left(\frac{l\pi}{H}\right)^2$ (l is an integer non null). Finally, the total electron eigenenergies in our structure can be written as:

$$E_{lmn}^e = \frac{m_e^*}{m_e^*(T)}\left[k_{mn}^2 + \left(\frac{l\,\pi}{H}\right)^2\right], \tag{13}$$

where $l = 1, 2, \cdots$ and $m = 0, \pm1, \pm2, \cdots$.

2.2. Thermodynamic properties

To study the thermodynamic properties of the system of electrons in cylindrical core/shell quantum dot we introduce the canonical partition function Z_c which gives a measure of thermally accessible states. It can be calculated by summation over all possible energy states. Following Boltzmann–Gibbs distribution, Z_c is provided by the well-known relation [37]:

$$Z_c = \sum_{\nu} e^{-\beta E_\nu} \tag{14}$$

where $\beta = 1/k_BT$ is the inverse temperature, k_B is the Boltzmann constant, T is the temperature expressed in Kelvin, and ν is the order of accessible energy levels E_ν such as $H|\nu\rangle = E_\nu|\nu\rangle$. Taking into account that the volume is constant, the mean energy of the system is given by the relation

$$\langle E\rangle = -\frac{\partial \ln Z_c}{\partial \beta}. \tag{15}$$

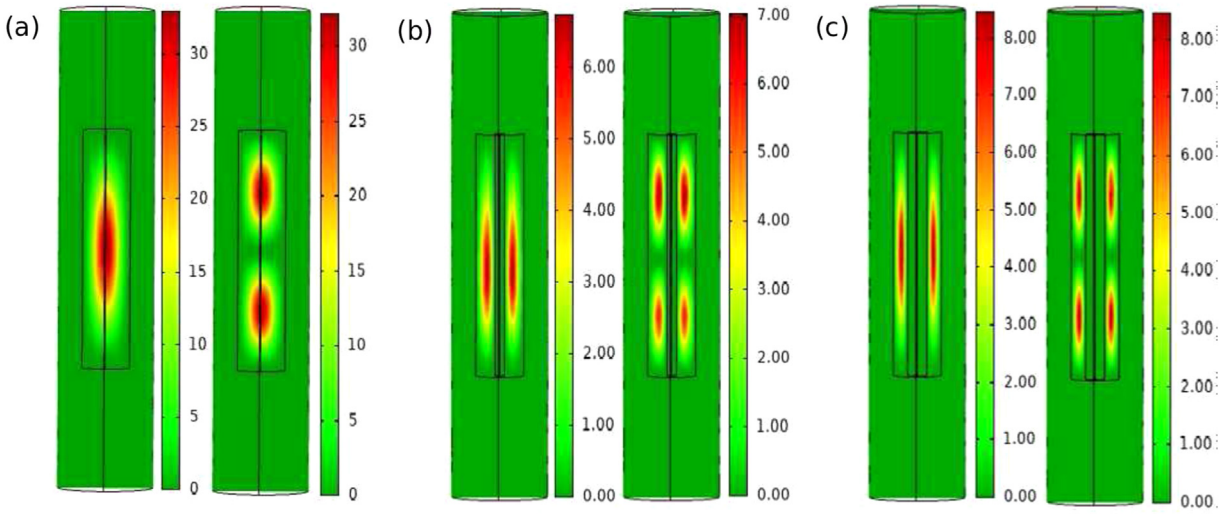


Fig. 2. Probability density of the two lowest confined states in GaAs cylindrical CSQD for $b = 1a^*$, $H = 10a^*$, and different values of core radius: (a) $a = 0$ ($L_w = 1a^*$), (b) $0.2a^*$ ($L_w = 0.8a^*$), and (c) $0.4a^*$ ($L_w = 0.6a^*$).

All thermodynamic properties of the system can be deduced from Z_c; in particular, the specific heat of the system which informs us about how much energy can be stored in the system per temperature degree increased. The relation gives:

$$C_V = -k_B\beta^2\left(\frac{\partial\langle E\rangle}{\partial\beta}\right) \tag{16}$$

The second crucial thermodynamic property is the entropy S, that gives the randomness in the system, it is defined by:

$$S = \frac{\langle E\rangle - F_H}{T}, \tag{17}$$

where $F_H = -\ln Z_c/\beta$ is the Helmholtz free energy, constituting the criterion of stability, and it is essential for studying the structure.

3. Results and discussions

In this work, numerical computations are done for systems as SnO_2/GaAs or SiO_2/GaAs nanofibers [44]. Given the difference of band gaps between core and shell material is sufficiently large ($E_g^{GaAs} = 1.42$ eV, $E_g^{SnO_2} = 3.68$ eV and $E_g^{SiO_2} = 9.8$ eV), so we can consider that the charge carriers are confined in the shell region [19]. From the experimental point of view, the deposition of the GaAs shell layers on the SnO_2 or SiO_2 by radio-frequency magnetron sputtering at low temperature is realized with better adhesion [44,51]. The scanning electron microscopy of the heterojunction cross-section shows high adherence and good morphological quality at the interfaces of SnO_2/GaAs or SiO_2/GaAs. This is why strain and defect induced by the mismatching could be neglected. The parameters of GaAs material used in this paper are given by: electron effective mass $m_e^*/m_0 = 0.063$, dielectric constant $\varepsilon = 13.18$, Bohr radius $a^* = \hbar^2\varepsilon/m_e^*e^2 = 11.07\ nm$, and effective Rydberg energy $R^* = \hbar^2/2m_e^*(a^*)^2 = 4.93$ meV [19]. Let us remark that he energy spectrum are determined by solving numerically the Eq. (10) using the software Maple [52]. Once all the energies are computed, they will be used to determine the partition function, which allow the determination of the thermodynamic quantities.

In order to study the confinement influence on the thermodynamic properties of the core/shell cylindrical quantum dot, we must analyze the effect of the two types of confinement: on the one hand, the size of the lateral dimension defined by the outer radius b (called 3D confinement) and on the other, the confinement domain represented by the shell (well) defined by the thickness $L_w = b - a$ (called 2D confinement) [53]. Our calculations are restricted for $L_w = 0.8,\ 0.6$ and $0.4a^*$ for a weak confinement $b = 3a^*$ (with $a = 2.2,\ 2.4$ and $2.6a^*$), and for strong confinement $b = 1a^*$ (with $a = 0.2,\ 0.4$ and $0.6a^*$). We note that in the case when $a = 0$, the thickness is $L_w = b$; which corresponds to the case of cylindrical GaAs QD. As it can be described in the theoretical part, the resolution of the transcendental Eq. (8), coupled with boundary conditions, allows to obtain the one particle energy.

First of all, we present in Fig. 2 the fundamental and the first excited state probability density amplitudes corresponding to $b = 1a^*$ and $H = 10a^*$. The horizontal axis corresponds to the radial direction, and the vertical axis corresponds to the revolution axis of the cylindrical dot. Three well thickness have been considered $L_w = 1,\ 0.8$, and $0.6a^*$ corresponding to core radii $a = 0,\ 0.2$ and $0.4\,a^*$, respectively. It can be observed that the increase of the core radius leads to the strong

Table 1
Partition function dependence (Z_c) on the number of energy levels (N) and the temperature for $b = 1a^*$.

L_w (a^*)	Z_c at $T = 100$ K			Z_c at $T = 300$ K		
	0.8	0.6	0.4	0.8	0.6	0.4
$N = 4$	2.385E−4	2.192E−7	5.539E−16	8.203E−2	7.886E−3	8.424E−6
6	2.385E−4	2.193E−7	5.540E−16	8.204E−2	7.890E−3	8.425E−6
10	2.385E−4	2.193E−7	5.540E−16	8.205E−2	7.891E−3	8.426E−6
12	2.385E−4	2.193E−7	5.540E−16	8.206E−2	7.891E−3	8.426E−6
15	2.385E−4	2.193E−7	5.540E−16	8.206E−2	7.891E−3	8.426E−6

Table 2
Partition function dependence (Z_c) on the number of energy levels (N) and the temperature for $b = 3a^*$.

L_w (a^*)	Z_c at $T = 100$ K			Z_c at $T = 300$ K		
	0.8	0.6	0.4	0.8	0.6	0.4
$N = 10$	4.566E−4	4.599E−7	1.184E−15	0.241	4.599E−5	2.291E−5
20	4.567E−4	4.600E−7	1.185E−15	0.2454	2.202E−2	2.292E−5
30	4.567E−4	4.600E−7	1.185E−15	0.2455	2.253E−2	2.293E−5
40	4.567E−4	4.600E−7	1.185E−15	0.2456	2.254E−2	2.293E−5
50	4.567E−4	4.600E−7	1.185E−15	0.2457	2.254E−2	2.293E−5

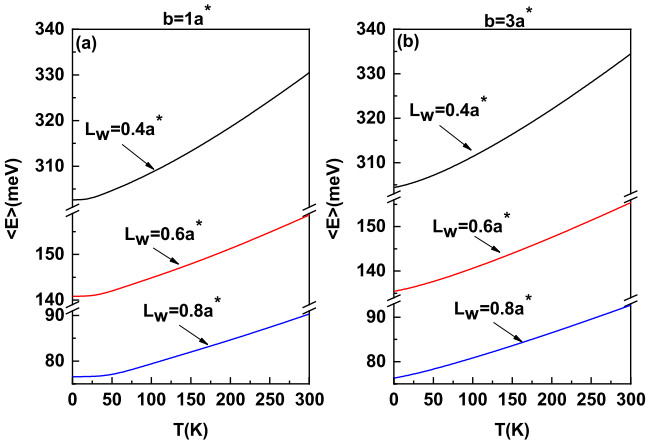


Fig. 3. Mean energies versus temperature for three shell thickness $L_w = 0.4,\ 0.6$, and $0.8a^*$, in the case of strong confinement $b = 1a^*$ (a), and for weak confinement $b = 3a^*$ (b).

radial squeezing of the electronic cloud. On the other hand, for the ground state, the maximum density of probability is symmetrically located in the median plane of the quantum cylinder, whatever the value of the thickness of the well. The electronic density of the first excited state, twice degenerate, is more localized for thin values of L_w. We note that the lowest value of L_w allows us to deduce quantitatively the tendency of a 2D system or nanotubes in which L_w can have atomic dimension.

Our numerical calculations of the partition function Z_c show that the saturation of the summation in the expression of Z_c depends on the shell (b) and the core (a) sizes, and also on the temperature (T). Table 1 presents Z_c for strong 3D-confinement ($b = 1a^*$), we remark that at $T = 100$ K and for $a = 0.2a^*$ and $a = 0.4a^*$, Z_c saturates from the 4th levels (by considering 9 digits) but for $a = 0.6a^*$ it saturates at 6th levels. However for $T = 300$ K the saturation is obtained at the end of more states, 13th levels what ever the value of the core size. Moreover, the weak 3D-confinement case is presented in Table 2 where we have presented our numerical calculation for ($b = 3a^*$). As we can remark at $T = 100$ K, the convergence of the summation of Z_c is obtained about the 20th state of all values of core sizes ($a = 2.2$, 2.4 and $2.6a^*$). At $T = 300$ K, Z_c saturates from the 43th, 30th, and 20th levels for $a = 2.2a^*$, $a = 2.4a^*$, and $a = 2.6a^*$, respectively.

Let us analyze the thermodynamic properties of this structure using the values of Z_c as a function of the temperature and of the two types of confinement taking into account the saturation values given in Tables 1 and 2. Fig. 3 shows the variations for mean energies as a function of the temperature: Fig. 3(a) corresponds to this variation in the strong 3D-confinement ($b = 1a^*$) and for $a = 0.2$, 0.4 and $0.6a^*$ which corresponds to shell thickness $L_w = 0.4$, 0.6 and $0.8a^*$ respectively. We remark that the mean energy of the system is still constant and stable until a $T = T_s$. This temperature decreases when the confinement thickness is reduced ($T_s = 31$ K for $L_w = 0.8$; 25 K for $L_w = 0.6$ and 17 K for $L_w = 0.4$). After T_s all curves increase almost linearly with temperature. On the other hand, in the case of the weak 3D-confinement ($b = 3a^*$) represented in Fig. 3(b), the energy of the system is very sensitive to the variation of temperature. Thus, for

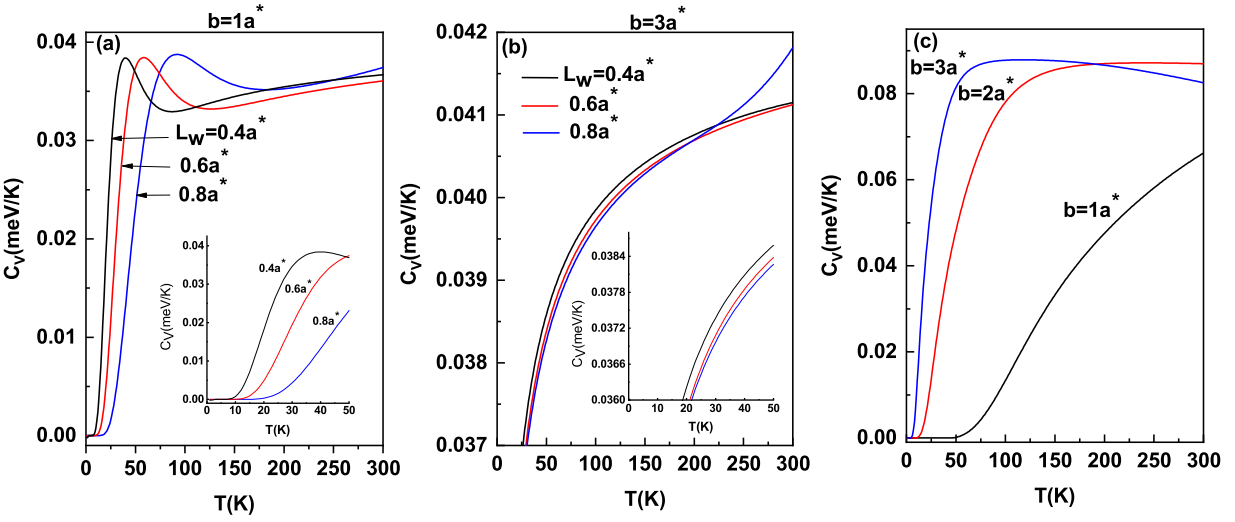


Fig. 4. Specific heat as function of temperature for three shell thickness $L_w = 0.4,\ 0.6$, and $0.8a^*$, in the case of: (a) strong 3D-confinement $b = 1a^*$, (b) weak 3D-confinement $b = 3a^*$ and (c) homogeneous cylindrical QD ($a = 0$) for three outer radii $b = 1,\ 2$ and $3\,a^*$. The insets are zoom for low temperature values.

the same well thickness $L_w = 0.4, 0.6$ and $0.8a^*$, the mean energy increases regularly with slopes depending on the well thickness which is in agreement with the physical properties of bulk semiconductors.

In Fig. 4 we present the variation of the heat capacity (C_v) as a function of the temperature for two confinement regimes $b = 1a^*$ and $b = 3a^*$ and for different values of the thickness: $L_w = (0.8, 0.6, 0.4)a^*$. Panel (a) of Fig. 4 corresponds to a strong confinement regime ($b = 1a^*$). We observe that for very low temperature ($T < 20$ K), the confinement effect has no influence on the specific heat, which remains negligible whatever the thickness of the well. By increasing the temperature, the QDs start to absorb the heat very fast, which explains the abrupt slope of the increasing heat capacity. Also, for critical values of T situated in the low temperature region ($T < 100$ K), (C_v) reaches maxima whatever the value of (L_w). This behavior is analogous to the Schottky anomaly encountered in the heat capacity of two-level systems at low temperature or due to the singlet–triplet transition in the ground state of QDs [33,36,37,41]. Besides, as it is indicated in the frame in panel (a), the threshold value T_s from which the CSQD starts to absorb the heat depends strongly on the values of the shell thickness. The specific heat shift peaks toward higher temperatures for low core radius (i.e., for large thickness L_w). Our calculation shows that for the used values of $L_w = 0.4, 0.6$, and $0.8a^*$, the peaks are obtained at $T = 39$ K, $T = 60$ K, and $T = 92$ K, respectively. The shapes of the peaks show a widening of the peaks when the shell thickness is reduced. A simple lecture of these curves shows that before the maximum, C_v is more important for narrow than wide well thickness. Indeed, the occupation density of the superior states decreases at low temperatures, but it increases with the enhancement of the quantum confinement. Consequently, the specific heat capacity depends on both effects: quantum confinement and temperature effects on the density of states. At low 3D confinement, the behavior of heat capacity undergoes a radical change: in the panel (b) of Fig. 4, we draw the variation of C_v for $b = 3a^*$ versus the temperature; a normal tendency to a saturation value of C_v for all values of L_w is observed. We note that at low temperature C_v is slightly superior for weak thickness dimension L_w as mentioned in the panel (b) of Fig. 4. To compare the previous conclusions with what happens in a homogeneous cylindrical QD (HCQD), which corresponds to $a = 0$, we draw in panel (c) of Fig. 4 the behavior of the specific heat for different HCQD radii ($b = 1,\ 2,$ and $3a^*$). As we can remark, the Schottky anomaly encountered in CSQD structure with strong 3D confinement at low temperature disappears and C_v admits a normal behavior as in bulk materials and tends to saturation values which increase at low confinement regime. Besides, for a given temperature, C_v becomes less important in strong confinement contrary to what happens in the case of CSQD indicated in Figs. 4(a) and 4(b), where the specific heat is reinforced in a strong 2D confinement regime (i.e., with decreasing L_w). Finally, let us remark that, by increasing the temperature, C_v tends to a saturation value. This result is in good agreement with the findings of Refs. [33,54,55].

In Fig. 5, we illustrate a 3D general mapping of the variation of the dependence of specific heat C_v as a function of both 2D confinement described by the thickness L_w and temperature T. We can see clearly that, for the case of strong 3D confinement, the Schottky anomaly is present whatever the strength of 2D confinement.

To analyze the behavior of the heat capacity deeply, we calculate its variations against the external QD size b for different values of temperature, as shown in Fig. 6. As we can remark, we can separate two regimes, for low values of b ($b < 1.6a^*$), the variation is very low compared to the weak confinement where $b > 1.6$. The increase is more pronounced when for $T > 100$ K.

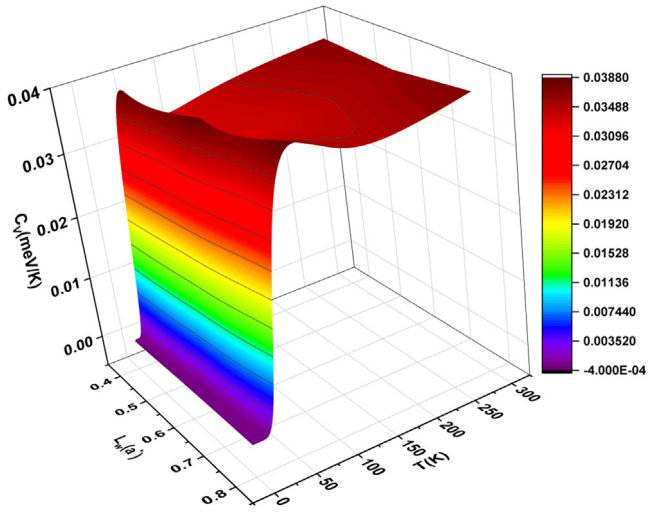


Fig. 5. 3D representation of the variation of the specific heat in cylindrical CSQD versus the thickness L_w and the temperature T.

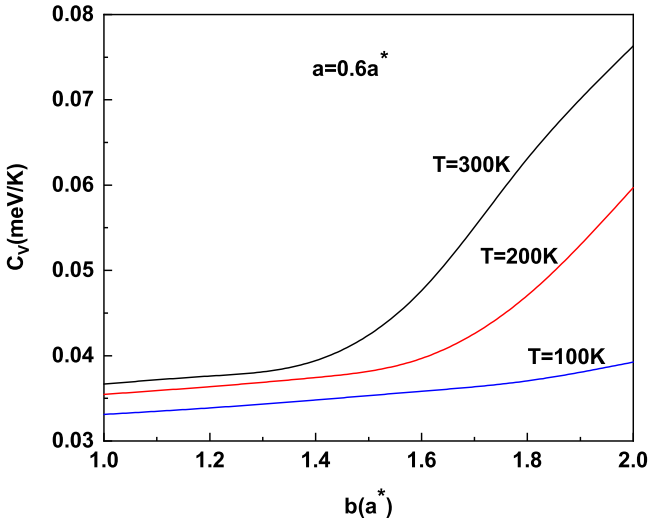


Fig. 6. Specific heat as a function of outer radius b for different values of temperature.

In Fig. 7 we present the variation of entropy S as a function of temperature. At very low temperature, this function, which determines the disorder of the system, tends to zero as it is predicted by thermodynamic laws. The entropy increases with increasing temperature because the occupation probability of levels changes and the system disorder is more important due to thermal agitation. Our calculation shows two important features: for small sizes ($b = 1a^*$), the entropy is very sensitive to the variation of the temperature as shown in Fig. 7(a). For a fixed temperature, the entropy becomes more important when we reduce the well thickness. Indeed, in strong confinement cases, the kinetic energy of particles becomes more important which leads to an augmentation of the system disorder.

As indicated in the inset of Fig. 7(a), the entropy admits fast variations at a low range of temperature 20 K $< T <$ 100 K whatever the value of the well widths. As one can see from Fig. 7(b), the entropy of a large dot size ($b = 3a^*$) increases with the temperature. At a given temperature, entropy increases with increasing quantum confinement effects. The behavior remains the same even for the low temperature, as shown the inset of Fig. 7(b). Our approach shows that for weak confinement, the entropy of the system keeps the same behavior for all value of temperature, whatever the well thickness. To give an idea concerning the variation of the entropy in HCQD, we present in Fig. 7(c) the variation of S against temperature, and for three significant radii values ($b = 1,\ 2,$ and $3\,a^*$). As it can be remarked, for a given QD radii b, S vary in the same manner as is CSQD. However, for a given T, the entropy is more pronounced for the weak confinement regime, contrary to what has been observed in the case of CSQD, indicated in Fig. 7(a) and Fig. 7(b), where the specific heat is reinforced in strong 2D confinement regime.

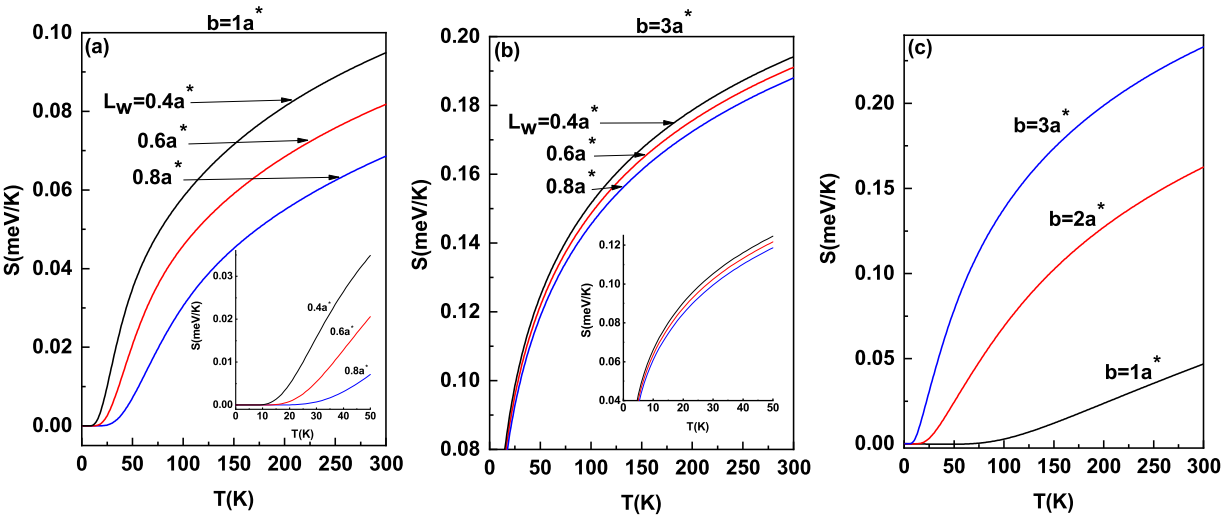


Fig. 7. Entropy versus temperature for three shell thickness $L_w = 0.4, 0.6$, and $0.8a^*$, in the case of strong confinement $b = 1a^*$ (a), and for weak confinement $b = 3a^*$ (b) and (c) represent the case of hollow cylindrical quantum dot for three outer radii $b = 1$, 2 and $3\,a^*$. The insets are zoom for low temperature values.

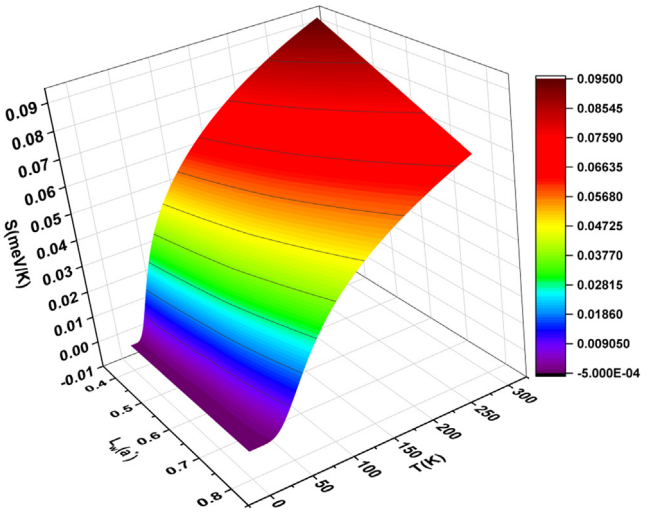


Fig. 8. Variations of the entropy in cylindrical CSQD versus the thickness L_w and the temperature T.

Fig. 8 gives the complete variation of S as a function of the parameters of the problem, where a 3D general mapping of the change of entropy S as a function of both 2D confinement through the thickness L_w and temperature T. To complete our analyze, we present Fig. 9 the variation of the entropy as function of the QD size for different values of the temperature. We observe that the entropy is increasing as function of the dot size and the temperature as well.

Finally, to investigate the stability of hollow cylindrical quantum dots, we present in Fig. 10 the Helmholtz free energy F_H drawn as a function of temperature for weak and strong confinement $b = 3a^*$ and $b = 1a^*$ respectively and for the same well thickness of the shell ($L_w = 0.4,\ 0.6$ and $0.8a^*$). Following the criterion of stability which postulates that a system is stable if itś Helmholtz energy is low. A simple lecture of our numerical results shows that F_H decreases when the temperature of the system increases whatever the dot sizes b and for all values of the well thickness L_w. The slope of different curves depends on two mode of confinements: outer radius (b) and also shell thickness (L_w). The different curves show a crossing at a low temperature ($T_c = 47$ K for $L_w = 0.8a^*$, $T_c = 36$ K for $L_w = 0.6a^*$ and $T_c = 28$ K for $L_w = 0.4a^*$) separating two regions indicating that F changes its behavior. For $T < T_c$ the function F_H is more important for large dot sizes than small sizes, so the strong confinement regime is more stable. This behavior is inverted for $T > T_c$, in this region the QD with weak confinement is more stable. The value of T_c tends to lower values for small widths of the well. From these ascertainment, we can deduce the existence of a competition between the effect of the temperature and the confinement. As we can see, the slope is more important for large outer radius and large well thickness. It can be

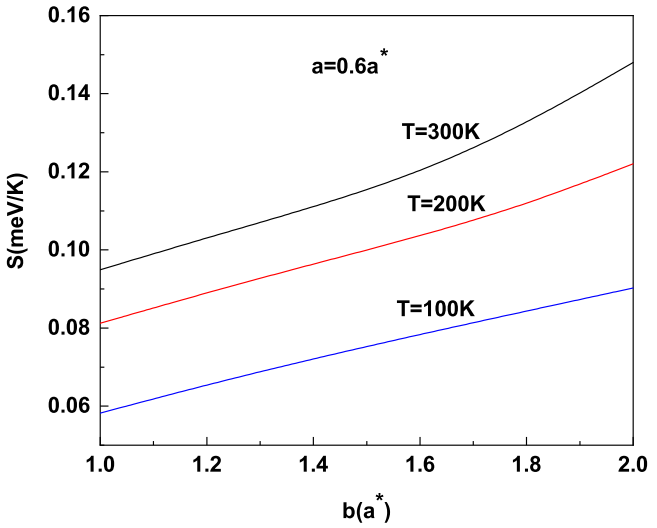


Fig. 9. Entropy as a function of outer radius b for different values of temperature.

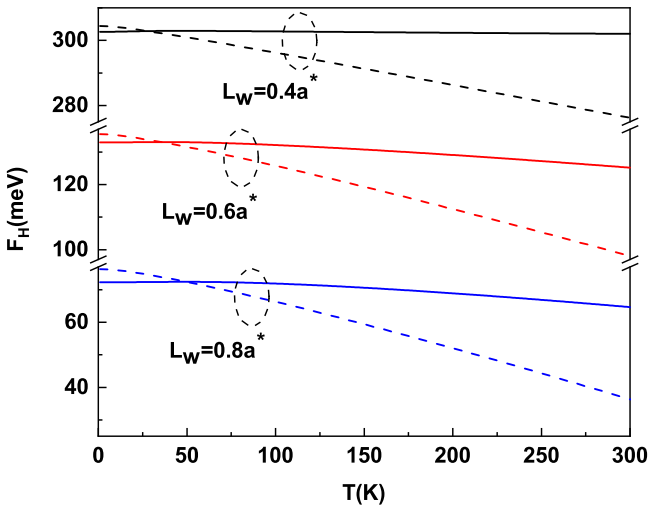


Fig. 10. Helmholtz free energy versus temperature for three shell thickness $L_w = 0.4, 0.6$, and $0.8a^*$, in the case of strong confinement $b = 1a^*$ (solid lines), and for weak confinement $b = 3a^*$ (dashed lines).

observed that for small dot sizes ($b = 1a^*$), the Helmholtz free energy diminishes slowly as the temperature (solid lines) is increased while the curvature of this energy is more pronounced for large dot size $b = 3a^*$ (dashed lines).

4. Conclusions

In this work, we have studied the evolution of the thermodynamic properties of cylindrical core/shell quantum dot as a function of both effects of confinement and temperature. Within the framework of the effective mass approximation, we solve analytically the Schrödinger equation in two bands models and we determine the energies of all excited states. Following Boltzmann–Gibbs distribution and introducing the canonical partition function, energy states are used to evaluate the mean energy, heat capacity, entropy, and Helmholtz free energy. Our numerical calculations show that all these thermodynamic properties depend on the temperature and on both lateral confinement and shell thickness. According to our results, the heat capacity shows a Schottky-like anomaly in low temperature for thin shells. The determination of Helmholtz free energy gives a quantitative idea about the evolution of the thermodynamic stability of quantum dots as a function of temperature and the confinement. Our study show that the competition between the 2D and 3D modes of confinement and the temperature influences the thermodynamic stability. Despite the simplicity of our approach, our study can be considered as a useful information source and a good qualitative indicator for understanding

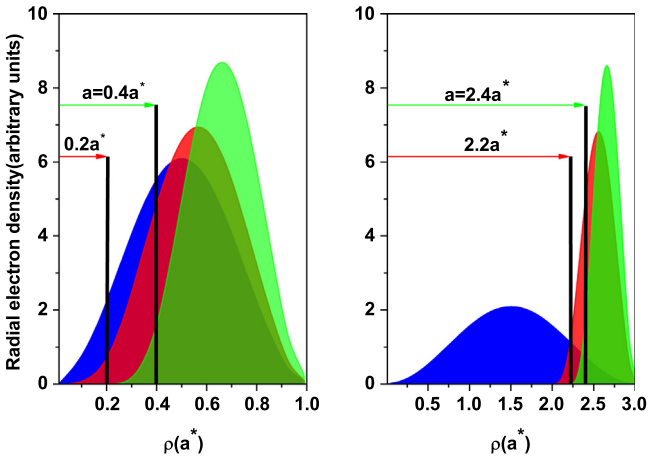


Fig. A.11. Radial probabilities of electron inside a core/shell with finite band offsets for two values of shell sizes: ($b = 1a^*$ with $a = 0, 0.2$ and $0.4a^*$) and ($b = 3a^*$ with $a = 0, 2.2$ and $2.4a^*$).

the thermodynamic properties of quantum dots. Finally, let us comment that the effect of finite potential in cylindrical core/shell quantum dot is a challenging problem that should be addressed, some preliminary results are shown in the Appendix, and the full calculations will be published in future works.

Declaration of competing interest

The authors declare that they have no known competing financial interests or personal relationships that could have appeared to influence the work reported in this paper.

Acknowledgments

We thank Prof. J.L. Bretonnet for his useful discussions. We thank to the anonymous reviewers, which helped us to improve the manuscript. LMP and DL acknowledge partial financial support from FONDECYT (Chile) 1180905. DL acknowledges partial financial support from Centers of excellence with BASAL/CONICYT financing (Chile), AFB180001, CEDENNA.

Appendix

Let us analyze in brief the effect of a finite confined potential. In the case of the finite band offsets, the radial part of Schrödinger equation of an electron confined in a cylindrical core/shell quantum dots can be written as:

$$\mathcal{H}_{\rho_e}\psi(\rho_e) = E_e\psi(\rho_e) \tag{A.1}$$

where the Hamiltonian, $\mathcal{H}_{\rho_e}$, is given by

$$\mathcal{H}_{\rho_e} = -\frac{\hbar^2}{2m_e^*}\nabla^2_{\rho_e} + V_w^e(\rho_e) \tag{A.2}$$

with

$$V_w^e(\rho_e) = \begin{cases} V_0 & \text{for} \quad \rho_e \le a \\ 0 & \text{for} \quad a \le \rho_e \le b \\ \infty & ; \quad \text{otherwise} \end{cases} \tag{A.3}$$

The analytical bound states solutions of the Eq. (A.1) can be cast in the form

$$\psi(\rho_e) = \begin{cases} AI_0(k_1\rho_e) & \text{if} \quad \rho_e \le a \\ B_1J_0(k_2\rho_e) + B_2Y_0(k_2\rho_e) & \text{if} \quad a \le \rho_e \le b \\ 0 & \text{if} \quad \rho_e > b \end{cases} \tag{A.4}$$

where $I_0(\rho_e)$ is the modified Bessel function, while $J_0(\rho_e)$ and $Y_0(\rho_e)$ are the Bessel functions of the first and second kind respectively. Here, A, B_1 and B_2 are the normalized constants. Finally, k_1 and k_2 are given by

$$k_1 = \sqrt{\frac{2m^*_{e(core)}}{\hbar^2}(V_0 - E_e)}; \quad k_2 = \sqrt{\frac{2m^*_{e(shell)}}{\hbar^2}E_e} \tag{A.5}$$

We remark that although the solution of the radial Schrödinger equation can be obtained analytically, the computations of the eigenvalues are more complicated. In Fig. A.11, we show the radial probability density as a function of the radial coordinate with the same fixed parameters as those used in the main text. We can clearly observe that the density is denser in shell with low extensions into the core region and vanishes at the border of the external region. Therefore, for this case, the infinite potential approximation treated in the manuscript is a good one, and can be used without any problem. More details of the finite potential effect will be published in future works.

References

[1] J.-J.S. De Groote, J. Hornos, A. Chaplik, Thermodynamic properties of quantum dots in a magnetic field, Phys. Rev. B 46 (19) (1992) 12773.
[2] T. Juntunen, T. Koskinen, V. Khayrudinov, T. Haggren, H. Jiang, H. Lipsanen, I. Tittonen, Thermal conductivity suppression in GaAs–AlAs core–shell nanowire arrays, Nanoscale 11 (43) (2019) 20507–20513.
[3] A.I. Boukai, Y. Bunimovich, J. Tahir-Kheli, J.-K. Yu, W.A. Goddard Iii, J.R. Heath, Silicon nanowires as efficient thermoelectric materials, Nature 451 (7175) (2008) 168–171.
[4] A.I. Hochbaum, R. Chen, R.D. Delgado, W. Liang, E.C. Garnett, M. Najarian, A. Majumdar, P. Yang, Enhanced thermoelectric performance of rough silicon nanowires, Nature 451 (7175) (2008) 163.
[5] E.K. Lee, L. Yin, Y. Lee, J.W. Lee, S.J. Lee, J. Lee, S.N. Cha, D. Whang, G.S. Hwang, K. Hippalgaonkar, et al., Large thermoelectric figure-of-merits from SiGe nanowires by simultaneously measuring electrical and thermal transport properties, Nano Lett. 12 (6) (2012) 2918–2923.
[6] J. Chen, G. Zhang, B. Li, Impacts of atomistic coating on thermal conductivity of germanium nanowires, Nano Lett. 12 (6) (2012) 2826–2832.
[7] M. Hu, X. Zhang, K.P. Giapis, D. Poulikakos, Thermal conductivity reduction in core-shell nanowires, Phys. Rev. B 84 (8) (2011) 085442.
[8] D. Mocatta, G. Cohen, J. Schattner, O. Millo, E. Rabani, U. Banin, Heavily doped semiconductor nanocrystal quantum dots, Science 332 (6025) (2011) 77–81.
[9] R. Wagner, W. Ellis, Vapor-liquid-solid mechanism of single crystal growth, Appl. Phys. Lett. 4 (5) (1964) 89–90.
[10] H. Zhou, I. Honma, H. Komiyama, J.W. Haus, Coated semiconductor nanoparticles; the cadmium sulfide/lead sulfide system's synthesis and properties, J. Phys. Chem. 97 (4) (1993) 895–901.
[11] A. Mews, A. Eychmüller, M. Giersig, D. Schooss, H. Weller, Preparation, characterization, and photophysics of the quantum dot quantum well system cadmium sulfide/mercury sulfide/cadmium sulfide, J. Phys. Chem. 98 (3) (1994) 934–941.
[12] J.W. Haus, H. Zhou, I. Honma, H. Komiyama, Quantum confinement in semiconductor heterostructure nanometer-size particles, Phys. Rev. B 47 (3) (1993) 1359.
[13] A. Kortan, R. Hull, R.L. Opila, M.G. Bawendi, M.L. Steigerwald, P. Carroll, L.E. Brus, Nucleation and growth of CdSe on ZnS quantum crystallite seeds, and vice versa, in inverse micelle media, J. Am. Chem. Soc. 112 (4) (1990) 1327–1332.
[14] O. Hayden, R. Agarwal, W. Lu, Semiconductor nanowire devices, Nano Today 3 (5–6) (2008) 12–22.
[15] D. Lucot, F. Jabeen, J.-C. Harmand, G. Patriarche, R. Giraud, G. Faini, D. Mailly, Quasi one-dimensional transport in single GaAs/AlGaAs core-shell nanowires, Appl. Phys. Lett. 98 (14) (2011) 142114.
[16] L.J. Lauhon, M.S. Gudiksen, D. Wang, C.M. Lieber, Epitaxial core–shell and core–multishell nanowire heterostructures, Nature 420 (6911) (2002) 57.
[17] P. Mohan, J. Motohisa, T. Fukui, Fabrication of InP/InAs/InP core-multishell heterostructure nanowires by selective area metalorganic vapor phase epitaxy, Appl. Phys. Lett. 88 (13) (2006) 133105.
[18] A. Fontcuberta i Morral, D. Spirkoska, J. Arbiol, M. Heigoldt, J.R. Morante, G. Abstreiter, Prismatic quantum heterostructures synthesized on molecular-beam epitaxy GaAs nanowires, small 4 (7) (2008) 899–903.
[19] M. El-Yadri, N. Aghoutane, A. El Aouami, E. Feddi, F. Dujardin, C. Duque, Temperature and hydrostatic pressure effects on single dopant states in hollow cylindrical core-shell quantum dot, Appl. Surf. Sci. 441 (2018) 204–209.
[20] E. Feddi, M. El-Yadri, F. Dujardin, R. Restrepo, C. Duque, Photoionization cross section and binding energy of single dopant in hollow cylindrical core/shell quantum dot, J. Appl. Phys. 121 (6) (2017) 064303.
[21] P. Mélinon, S. Begin-Colin, J.L. Duvail, F. Gauffre, N.H. Boime, G. Ledoux, J. Plain, P. Reiss, F. Silly, B. Warot-Fonrose, Engineered inorganic core/shell nanoparticles, Phys. Rep. 543 (3) (2014) 163–197.
[22] H.J. Fan, U. Gösele, M. Zacharias, Formation of nanotubes and hollow nanoparticles based on kirkendall and diffusion processes: a review, Small 3 (10) (2007) 1660–1671.
[23] S. Farsinezhad, T. Shanavas, N. Mahdi, A.M. Askar, P. Kar, H. Sharma, K. Shankar, Core–shell titanium dioxide–titanium nitride nanotube arrays with near-infrared plasmon resonances, Nanotechnology 29 (15) (2018) 154006.
[24] J. Xue, T. Wu, Y. Dai, Y. Xia, Electrospinning and electrospun nanofibers: Methods, materials, and applications, Chem. Rev. 119 (8) (2019) 5298–5415.
[25] M. Kria, M. El-Yadri, N. Aghoutane, L. Pérez, D. Laroze, E. Feddi, Forecasting and analysis of nonlinear optical responses by tuning the thickness of a doped hollow cylindrical quantum dot, Chinese J. Phys. 66 (2020) 444–452.
[26] B. Kelleher, D. Goulding, S. Hegarty, G. Huyet, E. Viktorov, T. Erneux, Optically injected single-mode quantum dot lasers, in: Quantum Dot Devices, Springer, 2012, pp. 1–22.
[27] E.U. Rafailov, M.A. Cataluna, E.A. Avrutin, Ultrafast Lasers Based on Quantum Dot Structures: Physics and Devices, John Wiley & Sons, 2011.
[28] H. Ortwin, G. Edeltraud, Photonics of Quantum-Dot Nanomaterials and Devices: Theory and Modelling, World Scientific, 2011.
[29] F. Zhou, A.L. Moore, M.T. Pettes, Y. Lee, J.H. Seol, Q.L. Ye, L. Rabenberg, L. Shi, Effect of growth base pressure on the thermoelectric properties of indium antimonide nanowires, J. Phys. D: Appl. Phys. 43 (2) (2009) 025406.
[30] S. Yazji, M.Y. Swinkels, M. De Luca, E. Hoffmann, D. Ercolani, S. Roddaro, G. Abstreiter, L. Sorba, E.P. Bakkers, I. Zardo, Assessing the thermoelectric properties of single InSb nanowires: the role of thermal contact resistance, Semicond. Sci. Technol. 31 (6) (2016) 064001.
[31] A. Mavrokefalos, A.L. Moore, M.T. Pettes, L. Shi, W. Wang, X. Li, Thermoelectric and structural characterizations of individual electrodeposited bismuth telluride nanowires, J. Appl. Phys. 105 (10) (2009) 104318.
[32] N.T. Nguyen, F. Peeters, Magnetic field dependence of the many-electron states in a magnetic quantum dot: The ferromagnetic-antiferromagnetic transition, Phys. Rev. B 78 (4) (2008) 045321.
[33] B. Boyacioglu, A. Chatterjee, Heat capacity and entropy of a GaAs quantum dot with Gaussian confinement, J. Appl. Phys. 112 (8) (2012) 083514.
[34] S. Gumber, M. Kumar, M. Gambhir, M. Mohan, P.K. Jha, Thermal and magnetic properties of cylindrical quantum dot with asymmetric confinement, Can. J. Phys. 93 (11) (2015) 1264–1268.
[35] S. Gumber, M. Kumar, P.K. Jha, M. Mohan, Thermodynamic behaviour of rashba quantum dot in the presence of magnetic field, Chin. Phys. B 25 (5) (2016) 056502.
[36] R. Khordad, H. Sedehi, Thermodynamic properties of a double ring-shaped quantum dot at low and high temperatures, J. Low Temp. Phys. 190 (3–4) (2018) 200–212.

[37] F. Nammas, Thermodynamic properties of two electrons quantum dot with harmonic interaction, Physica A 508 (2018) 187–198.
[38] F. Nammas, A. Sandouqa, H. Ghassib, M. Al-Sugheir, Thermodynamic properties of two-dimensional few-electrons quantum dot using the static fluctuation approximation (SFA), Physica B 406 (24) (2011) 4671–4677.
[39] K.L. Jahan, B. Boyacioglu, A. Chatterjee, Effect of confinement potential shape on the electronic, thermodynamic, magnetic and transport properties of a GaAs quantum dot at finite temperature, Sci. Rep. 9 (1) (2019) 1–10.
[40] D. Baghdasaryan, D. Hayrapetyan, E. Kazaryan, H. Sarkisyan, Thermal and magnetic properties of electron gas in toroidal quantum dot, Physica E 101 (2018) 1–4.
[41] M. Malik, S.K. Dandemraju, S. Mukhopadhyay, A. Chatterjee, Role of spin-orbit interactions on the entropy and heat capacity of a quantum dot helium placed in an external magnetic field, Physica E (2020) 114097.
[42] A. Alkauskas, P. Broqvist, F. Devynck, A. Pasquarello, Band offsets at semiconductor-oxide interfaces from hybrid density-functional calculations, Phys. Rev. Lett. 101 (10) (2008) 106802.
[43] D. Schooss, A. Mews, A. Eychmüller, H. Weller, Quantum-dot quantum well CdS/HgS/CdS: Theory and experiment, Phys. Rev. B 49 (24) (1994) 17072.
[44] L. Ghimpu, V. Ursaki, A. Pantazi, R. Mesterca, O. Brâncoveanu, S. Shree, R. Adelung, I. Tiginyanu, M. Enachescu, Characterization of core/shell structures based on CdTe and GaAs nanocrystalline layers deposited on SnO_2 microwires, Superlattices Microstruct. 116 (2018) 64–70.
[45] J.K. Yang, W.-S. Kim, H.-H. Park, Chemical bonding states and energy band gap of SiO_2-incorporated La2O3 films on n-GaAs (001), Thin Solid Films 494 (1–2) (2006) 311–314.
[46] W. Nakwaski, Effective masses of electrons and heavy holes in GaAs, InAs, A1As and their ternary compounds, Physica B 210 (1) (1995) 1–25.
[47] Z. Zeng, G. Gorgolis, C.S. Garoufalis, S. Baskoutas, Competition effects of electric and magnetic fields on impurity binding energy in a disc-shaped quantum dot in the presence of pressure and temperature, Sci. Adv. Mater. 6 (3) (2014) 586–591.
[48] S. López, N. Porras-Montenegro, C. Duque, Excitons in coupled quantum dots: hydrostatic pressure and electric field effects, Phys. Status Solidi b 246 (3) (2009) 630–634.
[49] C. Duque, S. López, M. Mora-Ramos, Hydrostatic pressure effects on the Γ–X conduction band mixing and the binding energy of a donor impurity in GaAs–$Ga_{1-x}Al_x$ quantum wells, Phys. Status Solidi b 244 (6) (2007) 1964–1970.
[50] M. Abramowitz, I. Stegun, Handbook of Mathematical Functions, Dover Publications, Inc., New York, 1970.
[51] D. Machado, L. Scalvi, A. Tabata, J.H. da Silva, Interface conduction and photo-induced electrical transport in the heterojunction formed by GaAs and Ce^{3+} doped SnO_2, J. Mater. Sci., Mater. Electron. 28 (2016) 1–10.
[52] https://www.maplesoft.com.
[53] J. El Khamkhami, E. Feddi, E. Assaid, F. Dujardin, B. Stébé, J. Diouri, Binding energy of excitons in inhomogeneous quantum dots under uniform electric field, Physica E 15 (2) (2002) 99–106.
[54] S.A. Mikhailov, Quantum-dot lithium in zero magnetic field: Electronic properties, thermodynamics, and fermi liquid–wigner solid crossover in the ground state, Phys. Rev. B 65 (11) (2002) 115312.
[55] H.-M. Müller, S. Koonin, Phase transitions in quantum dots, Phys. Rev. B 54 (20) (1996) 14532.